Cerebral Cortex Advance Access published February 20, 2013

Cerebral Cortex
doi:10.1093/cercor/bht040

Largely Typical Patterns of Resting-State Functional Connectivity in High-Functioning Adults with Autism

J. Michael Tyszka[1], Daniel P. Kennedy[2,3], Lynn K. Paul[2] and Ralph Adolphs[1,2]

[1]Division of Biology and [2]Division of Humanities and Social Sciences, California Institute of Technology, Pasadena, CA, USA and [3]Department of Psychological and Brain Sciences, Indiana University, Bloomington, IN, USA

Address correspondence to J. Michael Tyszka, 2A Broad 114-96, California Institute of Technology, 1200 E California Blvd, Pasadena CA 91125, USA. Email: jmt@caltech.edu; Dan Kennedy, Department of Psychological and Brain Sciences, Indiana University, 1101 E. 10th Street, Bloomington, IN 47405, USA. Email: dpk@indiana.edu

J. M. T and D. P. K. contributed equally to this work.

A leading hypothesis for the neural basis of autism postulates globally abnormal brain connectivity, yet the majority of studies report effects that are either very weak, inconsistent across studies, or explain results incompletely. Here we apply multiple analytical approaches to resting-state BOLD-fMRI data at the whole-brain level. Neurotypical and high-functioning adults with autism displayed very similar patterns and strengths of resting-state connectivity. We found only limited evidence in autism for abnormal resting-state connectivity at the regional level and no evidence for altered connectivity at the whole-brain level. Regional abnormalities in functional connectivity in autism spectrum disorder were primarily in the frontal and temporal cortices. Within these regions, functional connectivity with other brain regions was almost exclusively lower in the autism group. Further examination showed that even small amounts of head motion during scanning have large effects on functional connectivity measures and must be controlled carefully. Consequently, we suggest caution in the interpretation of apparent positive findings until all possible confounding effects can be ruled out. Additionally, we do not rule out the possibility that abnormal connectivity in autism is evident at the microstructural synaptic level, which may not be reflected sensitively in hemodynamic changes measured with BOLD-fMRI.

Keywords: autism spectrum disorder, functional magnetic resonance imaging, independent component analysis, resting-state networks, temporal correlation

Autism spectrum disorders (ASDs) affect ~1% of the population, yet their neural basis remains unknown. It is now clear that ASDs are complex and multigenic, and that divergent phenotypes can emerge from even identical genetic variations (Levitt and Campbell 2009; Geschwind 2011; State and Levitt 2011). The diagnosis "autism spectrum disorder" emphasizes the breadth of impairments seen and the wide range of their severity. Cognitive theories regarding the basic processing deficits seen in autism include social dysfunction (Hinsby et al. 2006), impaired global feature processing (Andersen et al. 2011), impaired reward processing (Chevallier et al. 2012; Damiano et al. 2012; Lin et al. 2012), motivation (Chevallier et al. 2012), and sensorimotor impairment (Perry et al. 2007).

One attractive hypothesis for reconciling this diversity of features is that autism is a generalized disorder of synaptic connectivity, with consequent effects on the functioning of distributed networks (Belmonte et al. 2004; Bourgeron 2009). This idea is supported by gains in our understanding of the genes implicated in autism, encoding cell adhesion and path-finding molecules (Glessner et al. 2009; Sbacchi et al. 2010), synapse proteins (Garber 2007), and neurotransmitter receptor function (Lee et al. 2002; Veenstra-VanderWeele et al. 2012). Arguably, the leading current hypothesis is that autism is a disease of abnormal connectivity and synapse formation in the brain, an abnormality that could explain both the ubiquitous neuroanatomical findings as well as the broad range of processing impairments.

Structural magnetic resonance imaging (MRI) reveals both increased (Herbert et al. 2004) and decreased (von dem Hagen et al. 2011) white matter volume across development in autism, as well as abnormal white matter microstructure (Barnea-Goraly et al. 2004; Weinstein et al. 2011). With functional MRI (fMRI), the most common finding in autism is decreased functional coupling between specific brain regions (Just et al. 2004; Koshino et al. 2005; Kleinhans et al. 2008). Functionally coupled regions exhibit spontaneous temporally correlated low-frequency oscillations in blood oxygenation-level–dependent (BOLD) signal that persist in the absence of any explicit task (i.e., during the resting state) and provide a comprehensive inventory of functional networks thought to reflect an underlying functional anatomy of the brain (Biswal et al. 2010).

Despite a flurry of recent resting-state functional connectivity MRI (rs-fcMRI) studies in autism (Anderson, Druzgal et al. 2011; Anderson, Nielsen et al. 2011; Di Martino et al. 2011; Ebisch et al. 2011; Gotts et al. 2012; von dem Hagen et al. 2012), results are surprisingly mixed (Muller et al. 2011). Studies have generally focused on a small number of brain regions or specific brain networks, so even when group differences have been reported the specificity of those findings to those particular regions or networks remains unclear.

Consequently, we took a whole-brain approach in high-functioning individuals with autism, compared with well-matched healthy controls, used multiple analysis methods, and examined in detail the effects of motion. Our aims were (1) to test at the whole-brain level the prevailing hypothesis that there is globally altered functional connectivity in autism, (2) to determine whether there is anatomical specificity to such putative abnormal connectivity, and (3) to explore the effects of head motion on the results.

Materials and Methods

Approach

There are 3 primary approaches to examining whole-brain resting-state connectivity: data-driven methods, anatomical-region of interest

(ROI), and functional-ROI analyses. Data-driven approaches are commonly implemented using independent component analysis (ICA), which derives spatiotemporally independent components that can then be compared across individuals and groups using a second-level analysis. The second approach, an anatomical ROI-based analysis, first parcellates the brain into distinct anatomical regions, determines the mean time series from each of these regions, and calculates temporal correlations in a pairwise manner, resulting in a large connectivity matrix. Functional-ROI connectivity analyses are typically, though not exclusively, used in task-based designs (Greicius et al. 2003) and were not employed in this study.

Each of these approaches has particular strengths and limitations (Joel et al. 2011). In anatomical ROI-based temporal correlation analysis, connectivity between specific regions is explicitly tested in a hypothesis-driven framework, for example, the strength of BOLD signal correlation between amygdala and ventral prefrontal cortex. However, individual patterns of activation are unlikely to conform exactly to atlas-based anatomical boundaries. The natural variation in the atlas region volume across the brain may also introduce biases, including signal interference from multiple sources within larger regions and poorer mean signal estimation in smaller regions. These concerns are mitigated in part by the use of probabilistic atlas regions and the use of multiple connectivity estimation approaches.

ICA is primarily an exploratory tool that attempts to decompose the observed resting-state BOLD signal into a set of maximally independent sources or components. The number of independent components must be estimated, generally either by inspection or by principle component analysis (Beckmann and Smith 2004) as used here. There is an increasing consensus regarding the characteristics of ICA-derived networks in the healthy brain, with stable spatial components reproduced across studies (Damoiseaux et al. 2006; Smith et al. 2009; Shirer et al. 2012). Hypothesis testing on these resulting components has historically proven difficult, but here we adopt an approach that employs dual-regression of the group-level IC temporal modes at the individual subject level, followed by conventional second-level analysis with statistical inference (Filippini et al. 2009). It has been established that both seed or ROI-based temporal correlation and independent component analyses provide complementary views of resting-state BOLD fMRI data (Joel et al. 2011) and together provide a more comprehensive picture of whole-brain connectivity than either does alone.

Subjects

Nineteen high-functioning adults with an ASD and 20 neurotypical controls with no family history of autism were recruited from our registry under a protocol approved by the Human Subjects Protection Committee of the California Institute of Technology. Diagnosis was confirmed by DSM-IV-R, and all participants with ASD met criteria on the Autism Diagnostic Observation Schedule (ADOS) (Lord et al. 2000) and Autism Diagnostic Interview-Revised (ADI-R) (Lord et al. 1994), the latter only when a caregiver was available ($n = 15$). We excluded participants with full-scale IQ < 80 or comorbid psychiatric or neurological conditions including but not limited to major depressive disorder, schizophrenia, epilepsy and history of traumatic brain injury. Controls were matched at the group level on age, sex, handedness and full-scale IQ (Table 1).

Medication Status

All subjects were screened for current and prior prescription and recreational or illegal drug use. Out of the 19 autism participants, 6 were taking one or more psychotropic medications: 1 was taking an SSRI (fluoxetine) for depressive symptoms, 2 were taking a stimulant (Adderall) for attentional issues, 1 was taking an anxiolytic (buspirone), 1 was taking a tricyclic antidepressant (amitriptyline) in addition to an atypical antipsychotic (risperidone) and the sixth was taking a stimulant (Ritalin) for attentional issues in addition to an anxiolytic (buspirone) and an SSRI (sertraline) for depressive symptoms. Of the 20 control participants, 1 was taking an SSRI (paroxetine) for depressive symptoms.

Table 1

Demographics, behavior, motion and structural statistics for autism and control groups

	Autism	Control	Test (df)	*P*
Sample size	19	20		
Fraction male	79%	84%	$\chi^2(1) = 0.099$	0.75
Age at scan (years)	27.4 (2.4)	28.5 (2.5)	$t_{(37)} = 0.32$	0.75
Behavior				
Fraction right handed	84%	80%	$\chi^2(1) = 0.008$	0.93
Verbal IQ	107.7 (3.6) [18]	113.9 (2.8)	$t_{(37)} = 1.37$	0.18
Performance IQ	107.4 (2.8) [18]	111.3 (2.2)	$t_{(37)} = 1.10$	0.28
Full-scale IQ	108.2 (3.0) [18]	114.1 (2.1)	$t_{(37)} = 1.64$	0.11
ADOS communication	4.4 (0.4)	—	—	—
ADOS reciprocal social interaction	9.1 (0.8)	—	—	—
ADI A	21.3 (1.3) [15]	—	—	—
ADI B	17.0 (1.0) [15]	—	—	—
ADI C	5.7 (0.7) [15]	—	—	—
ADI D	2.8 (0.4) [14]	—	—	—
SRS A	94.0 (7.6) [12]	—	—	—
EQ	24.4 (2.4) [17]	44.3 (4.6) [5]	$t_{(6)} = 3.78$	0.0091
Motion				
Mean F-F displacement (μm)	74.6 (9.4)	59.6 (5.3)	$t_{(37)} = 1.42$	0.17
Mean F-F rotation (millidegrees)	31.1 (2.7)	31.3 (2.7)	$t_{(37)} = 0.05$	0.96
Fraction of ICs classified as nuisance	57.2% (3.4%)	49.0% (3.7%)	$t_{(37)} = 1.63$	0.11
Variance explained by nuisance ICs	53.9% (3.5%)	46.2% (3.6%)	$t_{(37)} = 1.52$	0.14
Fraction of slices repaired	0.28% (0.12%)	0.02% (0.01%)	$U = 127.0$	0.04
Structure				
Mean within brain warping to MDA	0.318 (0.014)	0.299 (0.006)	$t_{(37)} = 1.31$	0.20

Where shown, values are mean (SEM) [sample size when different from group size]. All *t*-tests were two-tailed and unpaired, assuming equal variance. Chi-squared with Yate's correction was used to test differences in proportions (fraction male, right handed) and Mann–Whitney *U* was used to test differences in fractions of slices repaired.

Imaging

All MRI data were acquired using a 3 Tesla Magnetom Trio (Siemens Medical Solutions, NJ, USA) with an 8-channel phased array head receive coil and body coil transmission. Subjects were asked to lie still within the scanner with eyes closed, think of nothing specifically and to stay awake; all participants were accustomed to the scanner environment. Post-scan questioning confirmed a state of relaxed wakefulness in all participants. Two T_1-weighted MP-RAGE volumetric datasets were acquired as structural references (TR/TE/TI = 1590 ms/2.7 ms/800 ms, 1 average, 1 mm isotropic voxel size, total imaging time 7 min 26 s). The resting-state image acquisition consisted of 2 sessions of 5 min of T_2*-weighted single-shot echo planar imaging (EPI) (TR/TE = 2000/30 ms, flip angle = 75°, 2D multislice acquisition with 3.5 mm isotropic voxels, fat suppression, slices angled 30° axial-coronal relative to the main field). We adopted a resting-state session length of 5 min as it has been demonstrated that resting-state correlations stabilize by ~5 min even with a much longer TR (5 s vs. the 2 s used here) (Van Dijk et al. 2010). Two initial volumes (4 s) were discarded to reduce magnetization equilibration effects. Gradient echo field mapping data were acquired with identical geometry to the EPI data for EPI off-resonance distortion correction (TR/TE = 600/3.6 ms, 6.1 ms, flip angle = 60°). Resting-state fMRI data were acquired during a session in which no other functional tasks were performed; all other acquisitions during the session were structural acquisitions.

Minimum Deformation Atlas Construction

While the adult brain in autism is grossly similar to the neurotypical brain, numerous small differences are present (Abell et al. 1999; Ecker et al. 2012). We took care to minimize structural biases by first

estimating a Minimum Deformation Atlas (MDA) which minimizes the deformation required to map any one of the individual"s brain to the atlas template. The MDA was estimated using an iterative nonlinear registration approach similar to that proposed in MacKenzie-Graham et al. (2007) and employed previously in Tyszka et al. (2011). In an initial pass, both control and autism structural data were registered using FNIRT (Andersson et al. 2008) to the MNI152 1 mm whole-head T_1-weighted template. The average of all registered volumes became the template for the second pass. This process was repeated for a total of 4 passes, resulting in an estimated of the MDA closely aligned to the MNI152 space that was used as a registration template for all subsequent voxel-wise ICA and anatomical ROI segmentation analyses.

Preprocessing

Preprocessing was carried out using FEAT (v5.98) and MELODIC (v3.10), within FSL (FMRIB's Software Library, www.fmrib.ox.ac.uk/fsl). Transient artifacts were removed using ArtRepair with an outlier threshold of 5, automatic signal masking and per-slice correction by temporal linear interpolation (Mazaika et al. 2005). In 5 of the 19 autism subjects, only one session could be acquired due to participant tolerance or time constraints. To avoid bias associated with this missing data, all further analysis of both groups was restricted to a single session selected on the basis of lower number of transient artifacts identified by ArtRepair. No subject was excluded due to excessive transient artifacts; no session required more than 1.6% of slices to be repaired. Conventional preprocessing consisted of rigid-body motion correction, slice-timing correction, field map-based geometric distortion correction, nonbrain removal, and grand-mean intensity normalization. Finally, high pass temporal filtering was performed by subtraction of a local Gaussian-weighted least-squares straight-line fit with $\sigma = 50$s, comparable, but not equivalent, with traditional linear high pass filtering with a cut-off frequency of 0.01 Hz. No spatial smoothing was performed at this stage. Off-resonance geometric distortions in the EPI data were corrected using the PRELUDE and FUGUE toolboxes in FSL, using B_0 field maps derived from the dual-echo gradient echo dataset acquired with identical slice angle and voxel size to the EPI data. Nonbrain voxels were then masked, the data were demeaned and variance normalized on a voxel-wise basis.

In place of linear low pass filtering, which introduces additional temporal noise autocorrelation, nuisance ICs with broad frequency content were identified and removed at the single-subject level using an ICA-based approach. Individual subject ICs with more than 33% of the estimated spectral power in frequencies >0.1 Hz were removed from the time series, resulting in a cleaned, prefiltered dataset (Tyszka et al. 2011).

Finally, cleaned, prefiltered BOLD EPI data were registered to the MDA template in 2 steps: an initial affine registration to the T_1-weighted structural image, using the magnitude data from the field map as a proxy for the EPI space, and a nonlinear registration of the T_1-weighted structural image to the MDA template. EPI data were resampled in the MDA space at an isotropic spatial resolution of 3 mm. The same preprocessed data were used for both group-level ICA and region-based correlation analysis.

Atlas-based Inter-Regional Correlation

Functional connectivity reflected by temporal BOLD signal correlation was analyzed on signal time-series extracted from anatomically defined regions, together covering the entire cortex and subcortical regions in each subject. An additional 3 initial volumes were discarded to avoid driving correlations with residual equilibration effects. Gray matter, white matter, and cerebrospinal fluid (CSF) partial volume estimates (PVEs) were generated from each subject's T_1-weighted structural data using the FSL FAST tool (Zhang et al. 2001) and transformed to the MDA. For each subject, global nuisance signals derived from white matter and CSF time-courses were removed from the preprocessed BOLD time-series using a general linear model (GLM) approach described previously (Fox et al. 2009; Anderson, Druzgal et al. 2011). Individual subject GLMs were constructed with regressors constructed from mean signal time courses for the white matter PVE map and the ventricular CSF PVE map, each eroded by 4 mm. Finally, the 6 rigid body motion correction parameter time courses were added as motion confound regressors. The residual of this model, subsequently referred to as the corrected BOLD signal, was then used for inter-regional correlation analysis. Both cortical and subcortical regions were defined probabilistically using the Harvard-Oxford Atlas, co-localized to the MDA used in this study. The cortical labels in this atlas are ordered hierarchically, first by surface (lateral, medial, ventral, etc.) and then, where possible, by lobe, following the scheme proposed in Rademacher et al. (1992). A joint probabilistic mask was formed from the product of the individual gray matter PVE and atlas cortical region and used to weight the calculation of the mean signal from each subject's preprocessed BOLD time-course data.

Pearson's product–moment correlation coefficients were calculated for all pairs of atlas ROI time-courses, resulting in a 110×110 element symmetric interregional correlation matrix for each subject. All correlation coefficients within the matrix were Fisher z-transformed prior to subsequent statistical analysis. Group differences between the Fisher z matrices in their entirety were assessed by t-tests of each matrix element using false discovery rate (FDR) correction ($q = 0.05$) (Fig. 1*a*,*b*). In addition, elements corresponding to the 48 homotopic pairings were extracted from the correlation matrix and assessed for group differences with a nested 3-way ANOVA and post-hoc t-tests with FDR correction. Effect sizes are reported as Cohen's d for unpaired t-tests and η^2 (η_p^2) for variance explained by main effects and interactions in the analysis of variance.

Group comparisons of the distributions of correlations across the whole and subregions of the correlation matrix were performed by statistical inference on the parameters of a fitted model distribution at the individual subject level (Fig. 2*a*,*b*). Three analytic distributions (Student's t location-scale, gamma location-scale-shape, and generalized extreme value) were compared with Gaussian mixture modeling (GMM) with between 2 and 6 components using Bayes information criteria (BIC). GMM was strongly supported over analytical modeling, with 3 Gaussian components supported for the majority of individual subject correlation distributions. This support fell to 2 components for the majority of subjects at the subregion level. Consequently, for greater generality, a 2-component GMM fitted to both whole matrix and subregion correlation distributions (Fig. 1*c*). The 2 modeled Gaussian components represent the large number of low-correlation region-pairs and the smaller number of high, positive-valued correlations (e.g., homotopic correlations) in the matrix, respectively. Individual subject means for both Gaussians (μ_0 and μ_1) and the proportion of the lower Gaussian (p_0) were passed to a second-level analysis (unpaired t-test). All distribution modeling was performed using the Statistical Toolbox in Matlab R2011b (The Mathworks, Inc., Natick, MA, USA).

Motion Effects on Interregional Correlations

Recent studies have shed light on subject motion as a potentially significant source of bias in resting-state BOLD correlation studies (Power et al. 2012). We have attempted to address sources of bias arising from physiological pulsatility and gross, rigid body motion when looking at intergroup differences. As a second check, we compared interregional correlations between the 10 subjects with the highest and 10 subjects with the lowest mean displacement and rotational motion parameters derived from rigid body motion correction during preprocessing. Each motion group contained an equal number of ASD and control subjects and was therefore unbiased in terms of diagnosis.

Group ICA

A single group-level ICA (grand ICA) was performed across all subjects from both ASD and control groups using temporally concatenated probabilistic ICA (Calhoun et al. 2001). Probabilistic principal component analysis (PCA) was used to estimate the number of independent components supported by the data (Beckmann and Smith 2004). The whitened observations were decomposed into sets of vectors that describe signal variation across the concatenated subject-time domain,

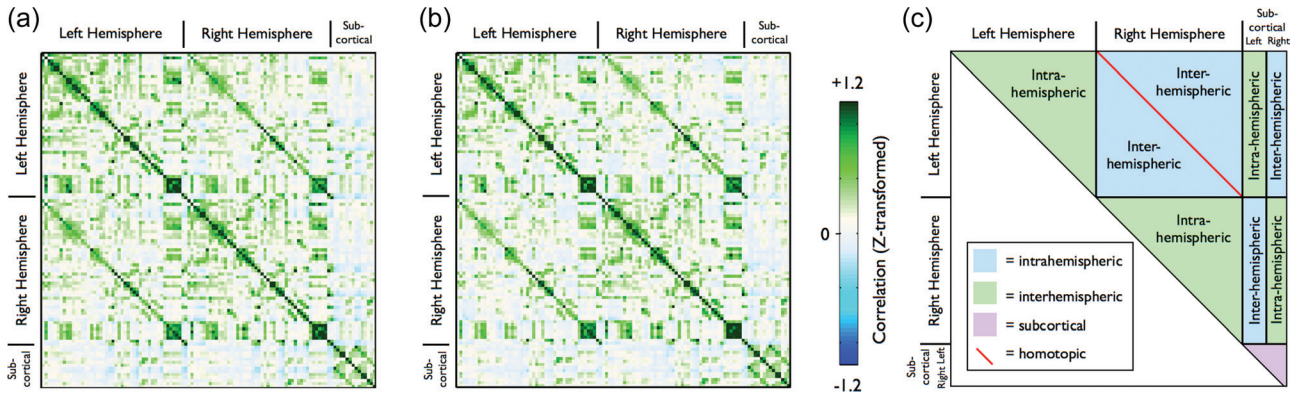

Figure 1. Atlas-based temporal coherence analysis. Interregional correlation matrices (Fisher *z*-transformed) for (*a*) controls ($n = 20$) and (*b*) autism subjects ($n = 19$). The correlation matrix can be divided into conventional connection families as shown in (*c*). Both group matrices show essentially identical patterns of correlation, reflected in the low residuals of the difference matrix. Strong homotopic correlations are evident in both cortical and subcortical sub-matrices. No individual pair-wise comparisons survived FDR control ($q = 0.05$). Note that these matrices are upper triangle symmetric. (*a* and *b*) are shown with identical scale limits. The row ordering within each hemisphere for the correlation matrices follows the surface-lobe hierarchy of the Harvard-Oxford atlas. Non-gray matter regions (white matter, CSF) and the brain stem are excluded from the subcortical regions.

and across the spatial domain by optimizing for non-Gaussian spatial source distributions. Estimated IC spatial maps were normalized to the standard deviation of the residual noise and thresholded at a false-discovery rejection rate of 95% for visualization purposes by fitting a mixture model to the histogram of intensity values (Beckmann and Smith 2004). Grand ICs associated with motion-by-magnetic field interactions at tissue-bone or tissue-air interfaces, or which were localized primarily in the white matter or CSF spaces, were classified by visual inspection using criteria suggested in Kelly et al. (2010) and excluded from further analysis.

Dual-regression and Group-level Inference

Voxel-wise group analysis of the ICA results was performed using the dual-regression approach described in Filippini et al. (2009). Dual-regression of the grand temporally concatenated ICA results was performed using scripts provided by the FSL toolbox (Madsen et al. 2004). In summary, dual-regression proceeds as follows: 1) Temporal modes for each grand IC are derived using a GLM with grand spatial modes as regressors. This results in single-subject time-courses corresponding to each of spatial components generated by the grand ICA over all subjects. 2) The temporal modes are normalized to unit variance. 3) The set of normalized individual temporal modes are used as regressors in a first-level GLM to derive individual subject spatial maps corresponding to each of the grand spatial maps. Finally, a second-level group analysis (i.e., ASD vs controls) is performed by nonparametric permutation testing on all single-subject spatial maps corresponding to each of the grand spatial ICs, and the between-subject group differences and consistencies derived. Second-level inference was thresholded at a family-wise error (FWE) corrected probability of 0.05 with threshold-free cluster-enhancement (TFCE) which provides both strong Type I and Type II error control (Madsen et al. 2003).

Results

Preprocessing Measures of Image Quality

Rigid-body motion correction parameters calculated during preprocessing were analyzed for group differences between ASD and control subjects. The frame-to-frame Euclidean displacement (Δr_{ff}) and total frame-to-frame angular rotation ($\Delta\theta_{ff}$) were chosen as measures of subject motion most likely to cause artifactual BOLD signal correlations. No significant between-group differences were observed in either metric and effect sizes were small to negligible. For frame-to-frame displacements, mean ± SEM Δr_{ff} was 60 ± 5 μm in controls and 75 ± 9 μm in ASD subjects ($t_{(37)} = 1.416$, $P = 0.1651$, unpaired *t*-test, equal variance). For frame-to-frame rotations, mean ± SEM $\Delta\theta_{ff}$ was 0.031 ± 0.003° in controls and 0.031 ± 0.003° in ASD subjects ($t_{(37)} = 0.051$, $P = 0.960$, unpaired *t*-test, equal variance). No significant between-group differences were observed in any of the preprocessing metrics, including total number of ICs, fraction of ICs considered nuisance components, variance explained by physiological ICs, or mean within-brain warping to the MDA template (Table 1).

Atlas-based Inter-regional Correlation

Taken as a whole, the mean correlation matrices calculated for autism and control groups were strikingly similar ($r = 0.97$, $P < 0.0001$) (Fig. 1*a*,*b*). Two-sample unpaired *t*-tests (equal variance) between autism and control correlations were run for each upper triangle element of the correlation matrix. No individual pair-wise tests survived FDR control ($q = 0.05$). In addition, between-group *t*-tests performed on whole-matrix Gaussian mixture model parameters revealed no significant group differences (μ_0: $P = 0.368$, Cohen's $d = 0.300$, μ_1: $P = 0.260$, Cohen's $d = 0.376$, p_0: $P = 0.261$, Cohen's $d = 0.375$) (Fig. 2*c*).

When correlation matrices were grouped based on motion rather than diagnosis, whole-brain differences between the correlation distributions for small and large motion groups appeared and were more pronounced than those due to diagnosis (Fig. 3). A very large, significant difference in the whole-matrix mixture model parameter μ_0 was observed between the high and low frame-to-frame rotation groups (unpaired *t*-test, $t_{(18)} = 3.36$, $P = 0.003$, Cohen's $d = 1.584$). A medium, but non-significant difference was observed in μ_0 for the large versus small displacement comparison (unpaired *t*-test, $t_{(18)} = 1.36$, $P = 0.191$, Cohen's $d = 0.641$). Both of these effect sizes were larger than that observed in μ_0 for the ASD versus control group comparison (Cohen's $d = 0.300$). Mean ± SEM frame-to-frame displacement, Δr_{ff}, was 113 ± 10 μm in the high-motion group and 37 ± 1 μm in the low-motion group ($t_{(18)} = 7.42$, $P < 0.0001$, unpaired *t*-test, equal variance). For frame-to-frame rotations, mean $\Delta\theta_{ff}$ was 0.047 ± 0.003°

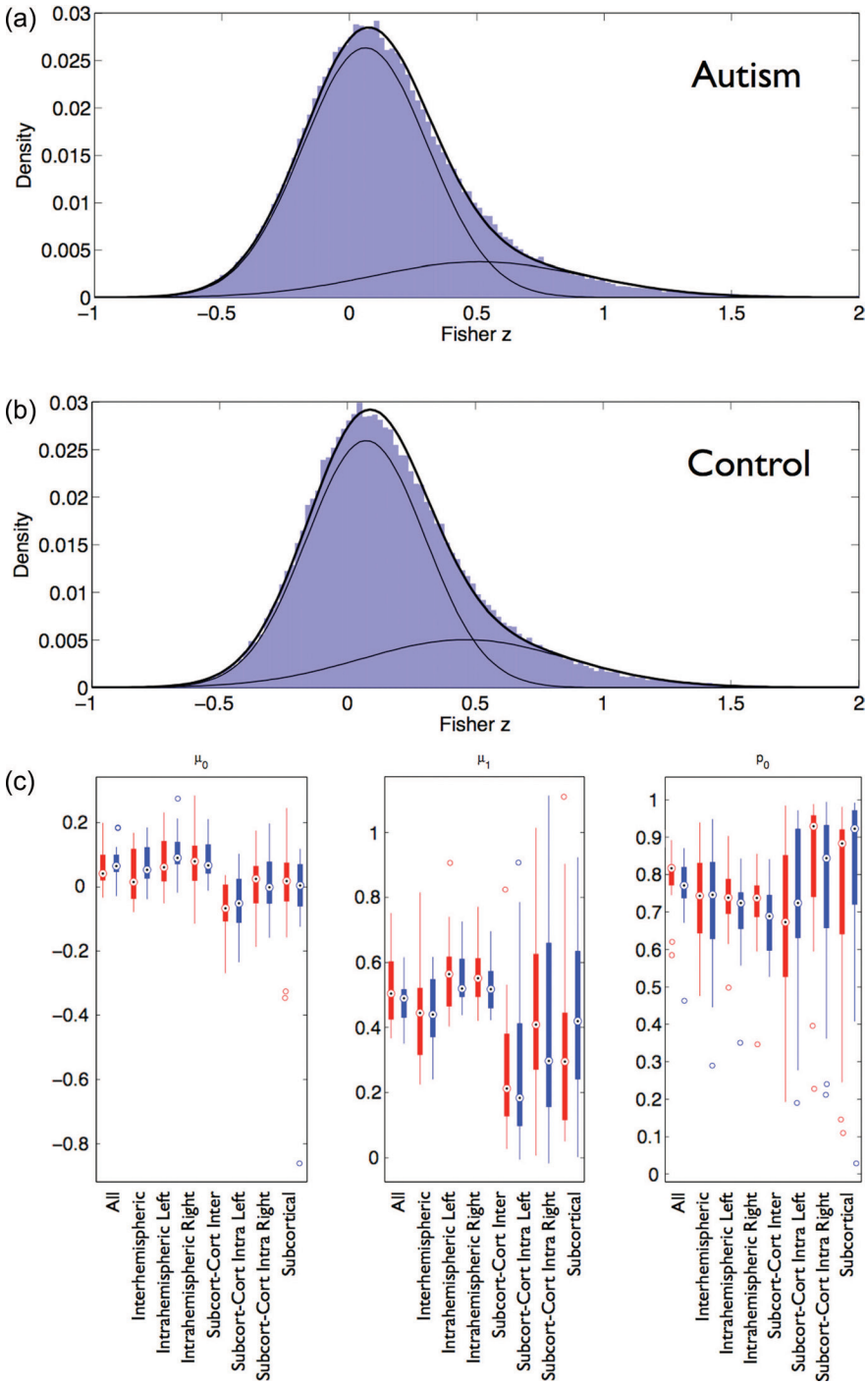

Figure 2. Two-component Gaussian mixture modeling example for all correlation matrix elements in (*a*) the control and (*b*) autism groups. (*c*) Comparison of mixture model means (μ_0, μ_1) and proportion (p_0) between autism (red) and controls (blue). No group differences survived FDR control ($q = 0.05$).

in the high-motion group and $0.019 \pm 0.001°$ in the low-motion group ($t_{(18)} = 10.4$, $P < 0.0001$, unpaired *t*-test, equal variance).

Gaussian mixture modeling of the correlation distributions for homotopic region pairs was precluded by the small sample size (48 region pairs) per subject. Instead, a 3-way ANOVA over region, subject and group was performed. Subjects were nested within group since individual subjects cannot cross between groups, and subject was treated as a random effect. There was a main effect of region ($F_{47,1739} = 65.91$, $P < 0.0001$, $\eta^2 = 0.555$), but no effect of group ($F_{1,37} = 0.300$, $P = 0.589$, $\eta^2 = 0.001$) or region × group interaction ($F_{47,1739} = 1.20$, $P = 0.172$, $\eta^2_p = 0.031$, $\eta^2 = 0.010$). In *post hoc* testing, only one of the 48 homotopic correlations was found to be significantly different between groups (two-sample *t*-test, $P = 0.036$) and this failed to survive correction for multiple comparisons (FDR correction with $q = 0.05$) (Fig. 4).

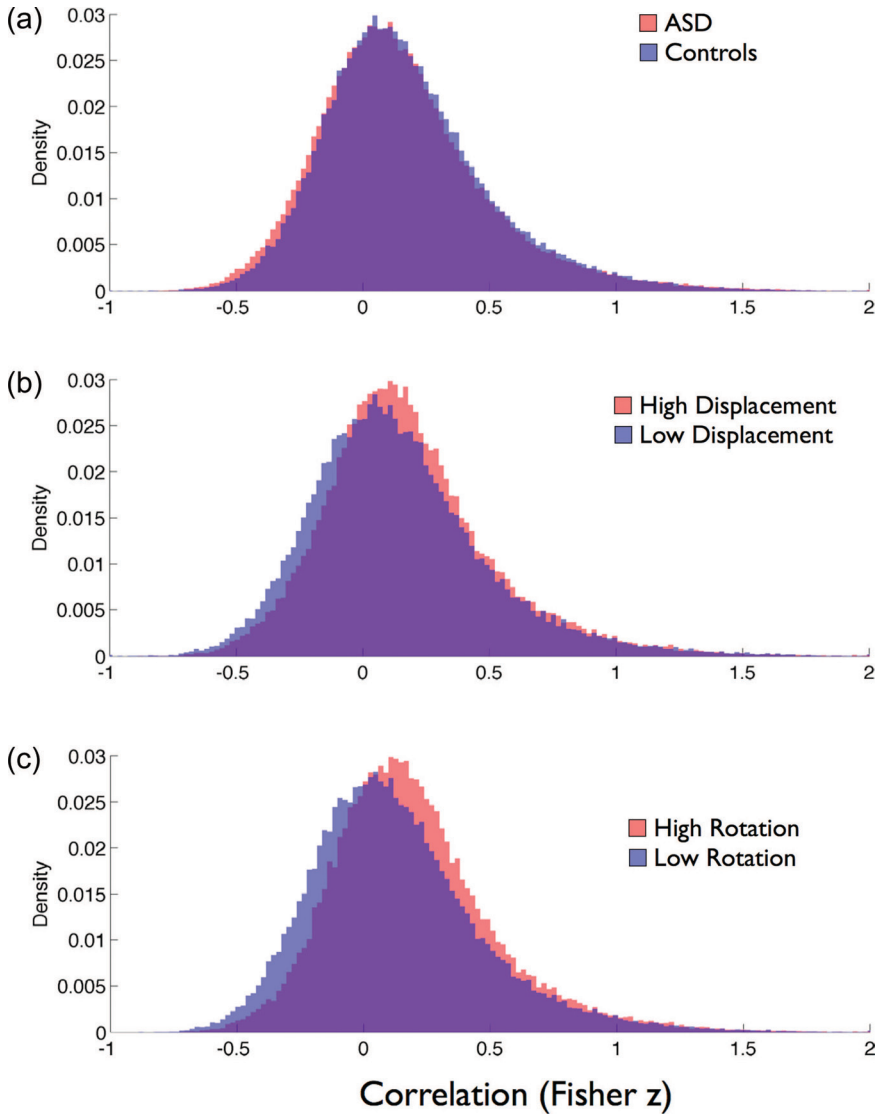

Figure 3. Normalized histograms of all correlations for (*a*) autism (red) versus controls (blue), (*b*) high (red) versus low (blue) translational motion groups and (*c*) high (red) and low (blue) angular motion groups. An equal number of autism and control subjects were included in each of the motion groups.

Although no single pair-wise correlations survived global FDR correction, abnormal patterns of correlations were apparent at the region level (i.e., across a given row or column of the correlation matrix) (Fig. 5). In order to assess this formally, the number of significantly different pair-wise correlations in each row was compared with that expected by chance at a Bonferroni-corrected probability of $0.05/110 = 0.00045$. Positive and negative pair-wise group correlation differences were analyzed separately. This corrected probability corresponded to 14 or more pair-wise correlations per row (using the cumulative binomial distribution). The following regions exhibited significantly high numbers of positive between-group differences (Control > ASD) when analyzed this way: Left frontal pole, left superior frontal gyrus, left middle frontal gyrus, left inferior frontal gyrus (Pars Opercularis), left temporal pole, left middle temporal gyrus (temporal–occipital part), left inferior temporal gyrus (temporal–occipital part), left angular gyrus, and left and right temporal fusiform cortex (posterior division). However, it should be kept in mind that temporal and frontal poles are regions of significant EPI signal dropout, making interpretation of findings in these 2 regions unclear. No significantly high counts of negative between-group differences were observed.

A supplementary analysis was performed in order to assess the impact of better matching the ASD and control groups on mean frame-to-frame motion. We excluded 2 subjects from the control group that had the least amount of movement, and 2 from the ASD group that had the greatest amount of motion. Following this procedure, groups were well matched on the mean levels of frame-to-frame displacement (autism: 65 ± 7 μm control: 62 ± 5 μm $t_{(33)} = 0.30$, $P = 0.760$). Group differences in the mean correlation matrices were analyzed as before, with very similar results. Minor differences were accounted for by some regions near threshold becoming significant, and others dropping slightly below significance. Overall, 7 of the 10 regions in the original analysis remained significantly different, suggesting that residual group differences in motion have only a minor effect on this analysis.

Independent Component Analysis

Temporally concatenated ICA over both ASD and control groups (grand ICA) yielded 43 components; of which, 23 were classified by inspection as neural in origin (Fig. 6). The remaining 20 components were made up of CSF-localized signal (3 of 20), Motion-by-field interactions (5 of 20), white matter-localized signals (6 of 20), and other non-neural cardiovascular signals (6 of 20). The 23 presumptive neural components can be assigned either directly or in combination with neurotypical components frequently observed in other resting-state BOLD fMRI studies (Table 2) (Smith et al. 2009; Shirer et al. 2012). Dual regression revealed essentially no between-group differences in networks identified by ICA (Fig. 7). There is some concern with temporally concatenated spatial ICA that grand ICs may be driven by a small number of subjects. However, the similarity of the dual regression group mean spatial maps (Fig. 7), both between groups and to the original grand spatial ICs (Fig. 6), suggests that these components are relatively consistent across subjects and not driven by outliers. No voxels in any component survived at an few-corrected probability of 0.05 in the second-level group analysis for the ASD > Control contrast. For the Control > ASD contrast, 16 voxels survived correction in component 16 but were located in white matter and 1 voxel survived in component 21. Taken together, no meaningful differences were detected by dual regression of group ICA results between ASD and control resting-states.

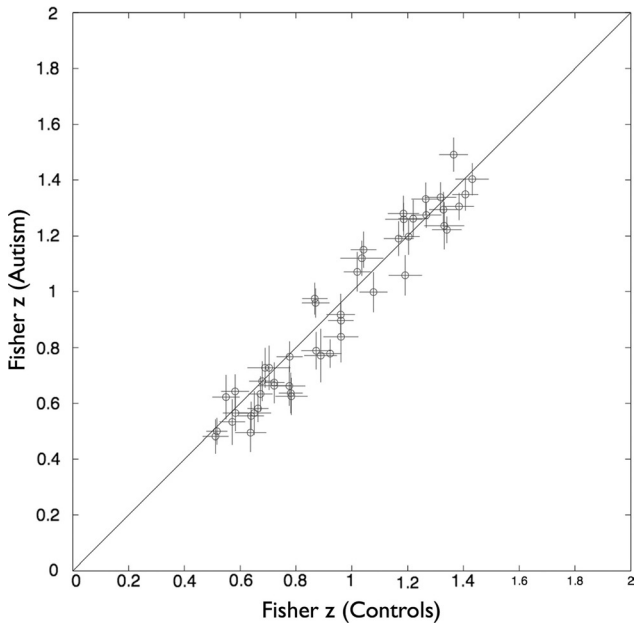

Figure 4. Scatterplot of homotopic *z*-transformed correlations for control and autism groups across all 48 regions. No significant between-group differences were observed following correction for multiple comparisons. Crosses indicate standard errors of the means for each group (control horizontal, autism vertical).

Discussion

In this study of high-functioning adults with autism, we find only limited evidence of abnormal connectivity at the regional level and no evidence at all for altered connectivity at the

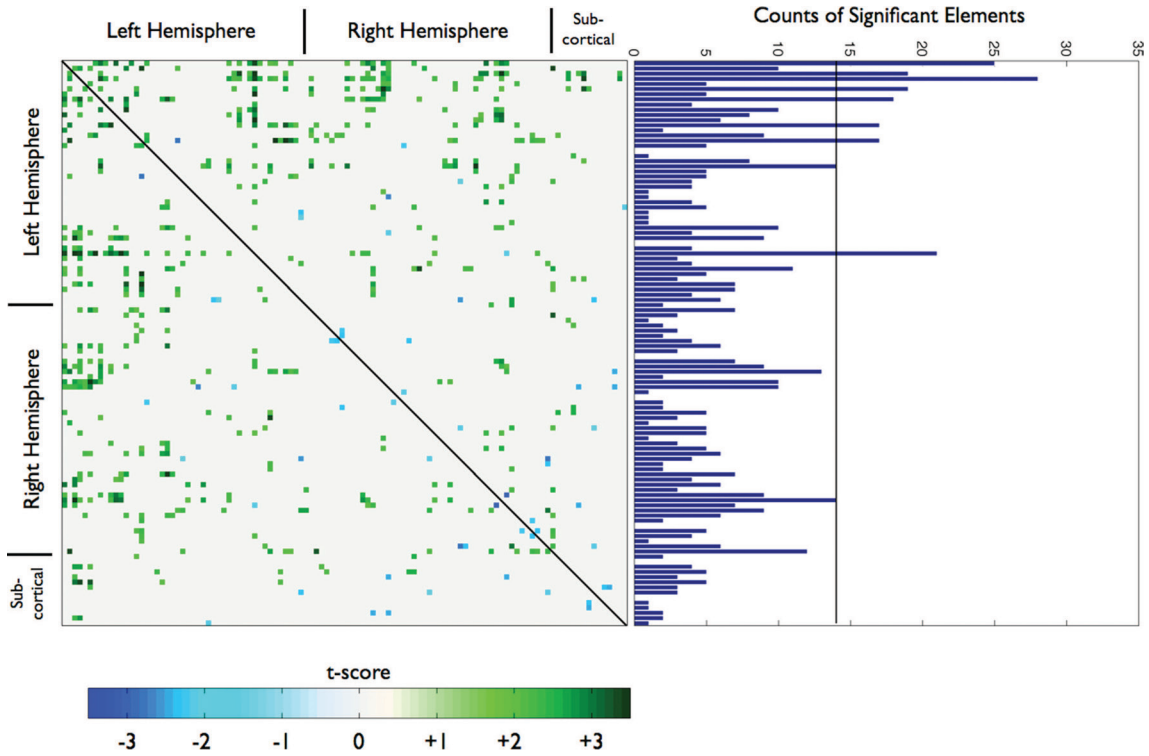

Figure 5. Thresholded t-map of regions that have significantly different pair-wise correlation between autism and control groups. The threshold is $P < 0.05$ with green indicating controls > autism and blue indicating autism > controls. The graph at right shows the total count of significantly positive group differences (control > autism) in each row of the correlation matrix. A region is identified as abnormal if the number of significantly different pair-wise correlations exceeds a Bonferroni-corrected threshold of 14 ($P < 0.05/110 = 0.00045$) with chance being 6. No significant counts of negative differences (autism > control) in each row were observed.

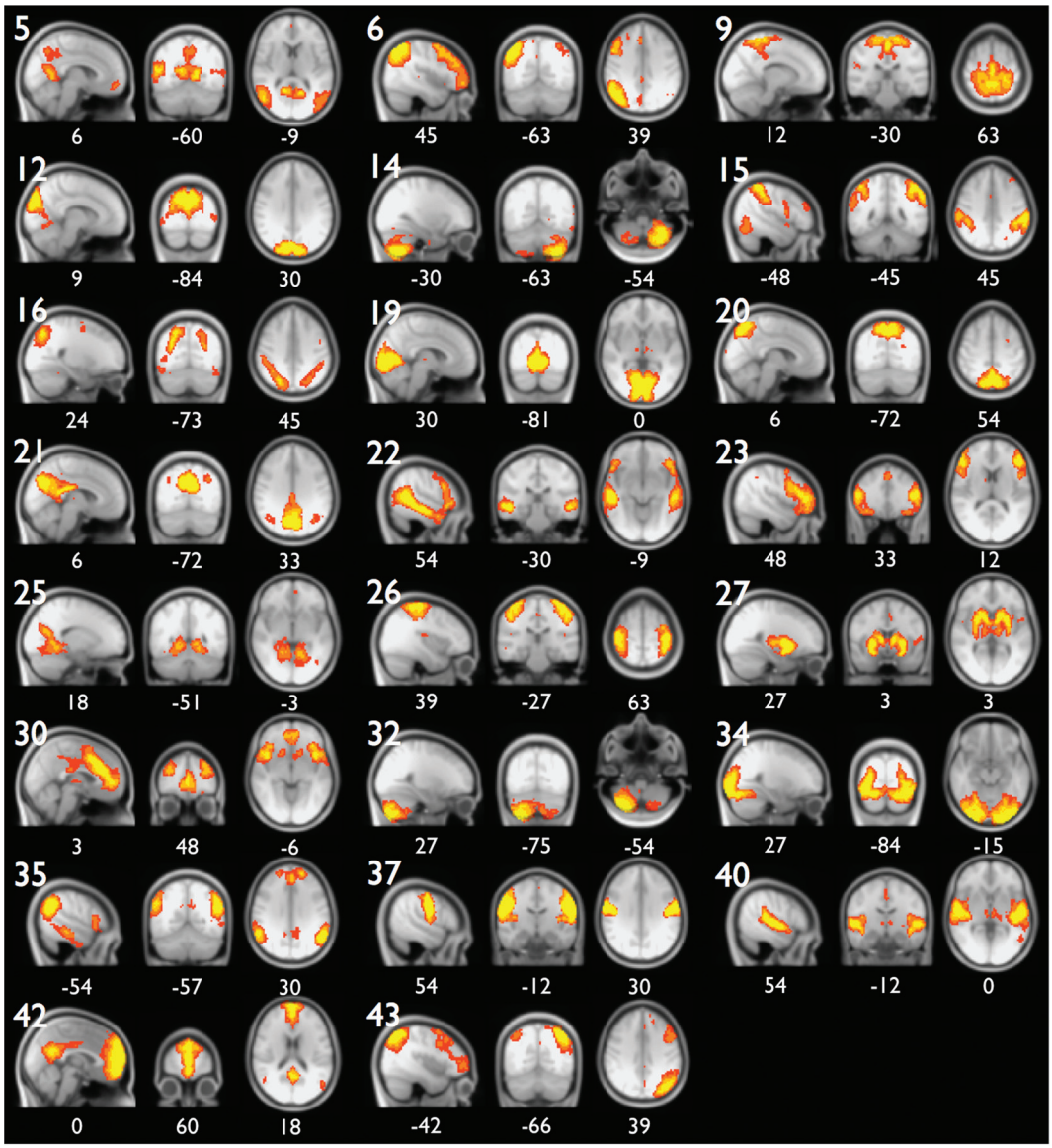

Figure 6. Spatial modes of the grand ICA over all subjects rank ordered by explained variance. Only neuronal ICs are shown for clarity. Tentative assignments for each spatial mode are listed in Table 2. MNI slice coordinates in mm are indicated below each image; sagittal slices with negative coordinates are within the left hemisphere.

whole-brain level. Regional abnormalities in functional connectivity in ASD were specific to particular brain regions within the frontal and temporal cortex (Fig. 5). Within these regions, functional connectivity with other brain regions was almost exclusively lower in the autism group. Our lack of global effects was bolstered by the use of 2 independent approaches: an anatomical ROI-based temporal correlation analysis and a data-driven ICA. Patterns and strength of temporal correlation illustrated by both methods showed a remarkable between-group similarity regardless of the type of connection, including interhemispheric (both heterotopic and homotopic), intrahemispheric, cortical–subcortical and subcortical, as well as at the network level. We paid careful attention to the control of motion artifacts and other non-neuronal confounds and also demonstrated that the residual effect of subject motion is larger than the effect of diagnosis.

These findings challenge the theory that the autistic brain is globally underconnected (Just et al. 2004). Recent refinements of the general underconnectivity theory in autism suggest that subnetworks such as frontal–parietal connections are particularly abnormal (Just et al. 2007; Minshew and Williams 2007). These theories and associated studies, however, tend to emphasize only the differences found between autism and neurotypical control groups, and deemphasize the similarities. We would argue that understanding the group similarities is just as important as understanding group differences, since both are necessary to inform a model of brain organization and functioning in autism. Below, we discuss the similarities identified in our study, and ask why such similarities have not been highlighted before.

One reason that similarities in functional connectivity are often not identified is that researchers generally have targeted brain regions or brain networks either thought to be or already known to be abnormal in autism, such as the default network (Cherkassky et al. 2006; Kennedy and Courchesne 2008; Monk et al. 2009; Assaf et al. 2010; Weng et al. 2010).

Table 2

Group-level neuronal-independent components identified over all subjects, percent of explained variance, functional/anatomical assignment and correspondence to neurotypical ICs described in Smith et al. (2009) and Shirer et al. (2012)

IC #	% Explained variance	Assignment	Corresponding IC in Smith et al. (2009)	Corresponding IC in Shirer et al. (2012)
5	4.30	Retrosplenial—lateral occipital	—	M (part)
6	4.16	Right parietal—dlPFC	9_{20}	K
9	3.40	Sensorimotor	6_{20} (part)	G (part)
12	3.12	Dorsal primary visual (V1)	I_{20} (part)	J (part)
14	2.92	Left cerebellum	5_{20} (part)	—
15	2.69	SMG—SPL	—	—
16	2.46	Interparietal sulcus	—	N (part)
19	2.05	Ventral primary visual (V1)	I_{20} (part)	J (part)
20	1.89	Dorsal precuneus	—	I (part)
21	1.85	Precuneus	—	I (part)
22	1.83	MTG—lateral prefrontal	—	E
23	1.79	Lateral prefrontal	—	—
25	1.61	Precuneus-lingual gyrus	—	—
26	1.45	Sensorimotor	6_{20} (part)	G (part)
27	1.37	Caudate-Putamen	—	B
30	1.06	Insula-dACC	8_{20}	L
32	0.82	Right cerebellum	5_{20} (part)	—
34	0.72	Secondary visual (V2)	3_{20}	D
35	0.71	DMN (parietal)	4_{20} (part)	C (part)
37	0.54	Lateral sensorimotor	6_{20} (part)	—
40	0.25	Primary auditory	7_{20}	A
42	0.49	DMN (medial)	4_{20} (part)	C (part)
43	1.45	Left parietal—DLPFC	10_{20}	F
Total	42.93			

DMN, Default Mode Network; dlPFC, dorsolateral prefrontal cortex; MTG, middle temporal gyrus; SMG, supramarginal gyrus; SPL, superior parietal lobule.

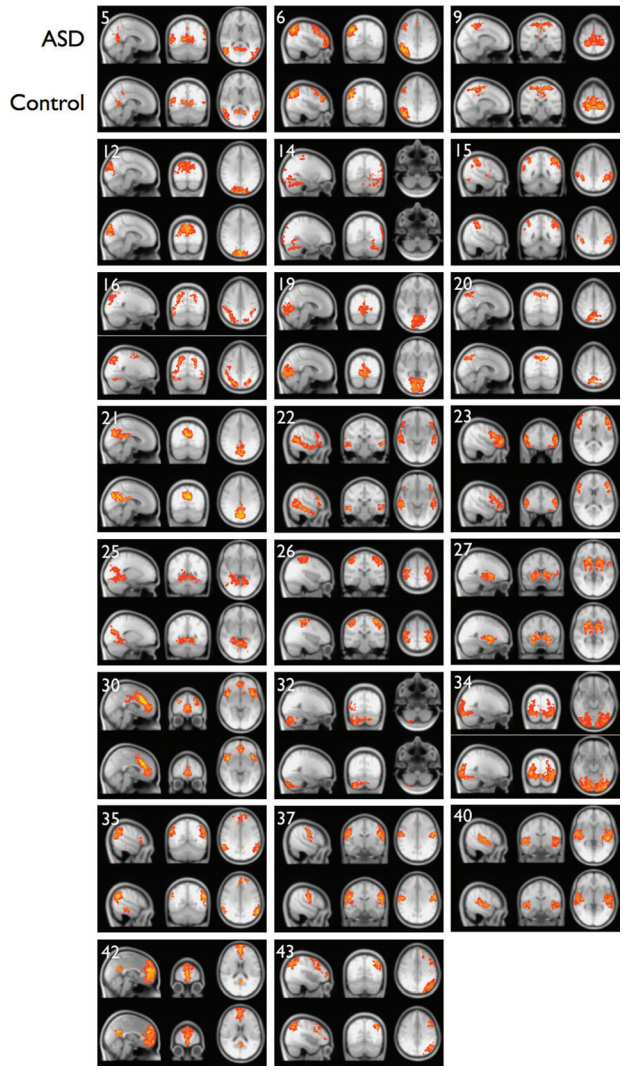

Figure 7. Group mean spatial maps for dual-regression of the 23 grand ICs to individual subjects demonstrating the between-group similarities. No meaningful between-group differences were observed for any grand IC. Slice locations for each IC are identical to those in Figure 6.

This can lead to the perception that the brain in autism is abnormally connected as a whole, although regions that might be expected to be typical in autism are largely ignored.

A second possible explanation for the overemphasis of group differences may be the context in which resting-state scans are acquired. First, the majority of studies exploring functional connectivity in autism do so in the context of a particular task (Just et al. 2004, 2007; Koshino et al. 2008). In some of these studies, the residual signal after regressing out the task time-course is used as a proxy for the resting-state (for review, see Muller et al. (2011)). However, the overlying tasks generally target cognitive processes that are thought to be difficult for individuals with autism (e.g., theory of mind, executive functioning, etc.), and by doing so, they are more likely to generate significant group differences in the proxy resting-state. Given the ease of acquisition, it is likely that many researchers simply add a resting-state scan to a larger task-based session. An earlier study by one of us identified reduced functional connectivity in autism between regions of the default network, but this resting-state scan was acquired immediately following scans asking participants to make self- and other-person judgments (Kennedy and Courchesne 2008). It is possible that the preceding task primed introspective cognitive processing differentially between the autism and control groups, influencing subsequent default network activity. Influences from prior tasks on resting-state activity have been reported for language tasks (Waites et al. 2005) and, more recently, in category-specific visual regions (Stevens et al. 2010). In our current study, resting-state scans were acquired only following task-free structural scans minimizing any task-based priming of our results. It is still possible that cognitive, attentional, and arousal differences could account for the regional differences that we did observe; if that was the case, then it is possible that the underlying functional architecture of autism is even more similar to typical controls than described here.

A third possible reason that prior studies have less often identified group similarities than group differences may be partly explained by group differences in the amount of head motion exhibited during scanning. Several recent reports emphasize careful control of gross motion effects in resting-state correlation analyses (Power et al. 2012; Van Dijk et al. 2012). This is especially important when comparing 2 different populations, such as children and adults or autism and controls, as different amounts of motion may be expected within each group. In addition, the effect of motion is not necessarily uniform for all brain regions and connection types. Greater

amounts of motion are thought to result in increased short-range and decreased long-range temporal correlations (Power et al. 2012).

Interestingly, this increased short-range and decreased long-range pattern has been postulated as a model for brain organization in autism (Courchesne and Pierce 2005), and so it will be necessary to see whether functional connectivity studies continue to lend support for this theory when methods that better account for motion are developed and used. In the present study, to determine how motion might affect our results, we show that both translational and rotational motions during scanning have a larger effect on measured correlations than does diagnosis (i.e., high-functioning autism vs. neurotypical controls). Furthermore, this large effect of motion was observed after attempting to control such effects at all levels of the preprocessing and analysis. This presents a major challenge for this type of research, but one that can hopefully be overcome through the development of new methods to deal with motion-related artifacts and careful consideration of how motion may impact one's results.

A fourth possible reason for the similarity observed between autism and controls is that this study is the composition of our participant sample (i.e., high-functioning adults). It is quite possible that effects would be more pronounced in younger and lower-functioning individuals. At least 1 study has suggested that altered functional connectivity may be more pronounced at younger ages (Anderson, Druzgal et al. 2011), but it is unclear whether motion was matched across groups and across the different ages in that study. We might speculate that in high-functioning adults with autism, near-typical patterns of functional connectivity are the result of plastic reorganization of brain networks, possibly resulting from many years of therapeutic intervention. In earlier work, we showed that typical organization of functional networks emerges even in the absence of a major anatomical pathway that normally supports typical network functioning (Tyszka et al. 2011). That study found that individuals with agenesis of the corpus callosum (a congenital condition where the fibers of the corpus callosum fail to cross the midline) still showed the normal complement of resting-state networks, and even exhibited the same level of functional connectivity between homotopic regions of the left and right cerebral cortices. Thus, the emergence of these resting-state networks is remarkably resilient to early developmental perturbation, perhaps more so than anyone may have thought was previously possible. Furthermore, we might speculate that those individuals who are best able to respond to the demands of their environment (the so-called high-functioning individuals, such as those included in the present study) are those that were able to establish typical neural networks. This remains an open but testable question.

A final reason for the lack of emphasis on similarity is a positive publication bias towards differences between groups, a broad problem in scientific publication that has received considerable recent attention (Johnson and Dickersin 2007; Bennett et al. 2009; Jennings and Van Horn 2012). As more studies are being published and more data are being generated and analyzed, it is becoming clear that a useful description of functional connectivity in autism must be more nuanced than simply under-connected or over-connected (Anderson, Nielsen et al. 2011; Muller et al. 2011). Whatever that the outcome may be, our present findings suggest that the effect size is small, and in particular that it is smaller than residual effects of head motion in the scanner.

This study has some limitations, most notably that the sample size is relatively small. The advent of data-sharing platforms such as the Autism Brain Imaging Data Exchange (ABIDE) and the National Database for Autism Research (NDAR) open up the possibility of extending this analysis to larger groups of subjects (including younger participants with autism), providing better Type II (False Negative) error control than that could be achieved here. Relatedly, larger sample sizes will allow for better group-level matching on psychotropic drug use. Although we believe that this factor is unlikely to have accounted for our results, especially given the high degree of similarity of the correlation distributions between groups (Fig. 2), we cannot conclusively rule out this possibility. Additional studies that disentangle the effects of psychotropic drugs on resting state functional connectivity will be necessary.

In conclusion, this study finds support for abnormal brain connectivity in ASD at the regional level only in a limited set of frontal and temporal cortical regions. No significant differences were observed at the whole-brain level between ASD and control groups using atlas-based regional correlation or group ICA analysis of BOLD RSNs. Most importantly, group differences between the subjects demonstrating the most and least motion during the fMRI acquisition were more significant than those seen between ASD and control groups.

Funding

This work was supported by a Conte Center grant from the National Institutes of Health (P50MH094258 to R.A., J.M.T., L. K.P.) and grants from the Simons Foundation (SFARI-07-01 to R.A.), the National Institutes of Health (R01 MH080721 to R. A.; K99MH094409/R00MH094409 to D.P.K.), and the National Alliance for Research on Schizophrenia and Depression (2009 Young Investigator Award to L.K.P.).

Notes

The authors wish to thank Catherine Holcomb for all her administrative efforts in support of this project. Conflict of interest: none declared.

References

Abell F, Krams M, Ashburner J, Passingham R, Friston K, Frackowiak R, Happe F, Frith C, Frith U. 1999. The neuroanatomy of autism: a voxel-based whole brain analysis of structural scans. Neuroreport. 10:1647–1651.

Andersson JL, Smith S, Jenkinson M. 2008. FNIRT–FMRIB non-linear image registration tool. 14th Annual Meeting of the Organization for Human Brain Mapping, Melbourne, Australia. 496 p.

Anderson JS, Druzgal TJ, Froehlich A, Dubray MB, Lange N, Alexander AL, Abildskov T, Nielsen JA, Cariello AN, Cooperrider JR et al. 2011. Decreased interhemispheric functional connectivity in autism. Cereb Cortex. 21:1134–1146.

Anderson JS, Nielsen JA, Froehlich AL, DuBray MB, Druzgal TJ, Cariello AN, Cooperrider JR, Zielinski BA, Ravichandran C, Fletcher PT et al. 2011. Functional connectivity magnetic resonance imaging classification of autism. Brain. 134:3742–3754.

Andersen LM, Naswall K, Manouilenko I, Nylander L, Edgar J, Ritvo RA, Ritvo E, Bejerot S. 2011. The Swedish version of the Ritvo

autism and asperger diagnostic scale: revised (RAADS-R). A validation study of a rating scale for adults. J Autism Dev Disord. 41:1635–1645.
Assaf M, Jagannathan K, Calhoun VD, Miller L, Stevens MC, Sahl R, O'Boyle JG, Schultz RT, Pearlson GD. 2010. Abnormal functional connectivity of default mode sub-networks in autism spectrum disorder patients. Neuroimage. 53:247–256.
Barnea-Goraly N, Kwon H, Menon V, Eliez S, Lotspeich L, Reiss AL. 2004. White matter structure in autism: preliminary evidence from diffusion tensor imaging. Biol Psychiatry. 55:323–326.
Beckmann CF, Smith SM. 2004. Probabilistic independent component analysis for functional magnetic resonance imaging. IEEE Trans Med Imaging. 23:137–152.
Belmonte MK, Allen G, Beckel-Mitchener A, Boulanger LM, Carper RA, Webb SJ. 2004. Autism and abnormal development of brain connectivity. J Neurosci. 24:9228–9231.
Bennett CM, Wolford GL, Miller MB. 2009. The principled control of false positives in neuroimaging. Soc Cogn Affect Neurosci. 4:417–422.
Biswal BB, Mennes M, Zuo XN, Gohel S, Kelly C, Smith SM, Beckmann CF, Adelstein JS, Buckner RL, Colcombe S et al. 2010. Toward discovery science of human brain function. Proc Natl Acad Sci USA. 107:4734–4739.
Bourgeron T. 2009. A synaptic trek to autism. Curr Opin Neurobiol. 19:231–234.
Calhoun VD, Adali T, Pearlson GD, Pekar JJ. 2001. A method for making group inferences from functional MRI data using independent component analysis. Hum Brain Mapp. 14:140–151.
Cherkassky VL, Kana RK, Keller TA, Just MA. 2006. Functional connectivity in a baseline resting-state network in autism. NeuroReport. 17:1687–1690.
Chevallier C, Kohls G, Troiani V, Brodkin ES, Schultz RT. 2012. The social motivation theory of autism. Trends Cogn Sci. 16: 231–239.
Courchesne E, Pierce K. 2005. Why the frontal cortex in autism might be talking only to itself: local over-connectivity but long-distance disconnection. Curr Opin Neurobiol. 15:225–230.
Damiano CR, Aloi J, Teadway M, Bodfish JW, Dichter GS. 2012. Adults with autism spectrum disorders exhibity decreased sensitivity to reward parameters when making effort-based decisions. J Neurodevelop Disord. 4:13.
Damoiseaux JS, Rombouts SA, Barkhof F, Scheltens P, Stam CJ, Smith SM, Beckmann CF. 2006. Consistent resting-state networks across healthy subjects. Proc Natl Acad Sci USA. 103:13848–13853.
Di Martino A, Kelly C, Grzadzinski R, Zuo XN, Mennes M, Mairena MA, Lord C, Castellanos FX, Milham MP. 2011. Aberrant striatal functional connectivity in children with autism. Biol Psychiatry. 69:847–856.
Ebisch SJ, Gallese V, Willems RM, Mantini D, Groen WB, Romani GL, Buitelaar JK, Bekkering H. 2011. Altered intrinsic functional connectivity of anterior and posterior insula regions in high-functioning participants with autism spectrum disorder. Hum Brain Mapp. 32:1013–1028.
Ecker C, Suckling J, Deoni SC, Lombardo MV, Bullmore ET, Baron-Cohen S, Catani M, Jezzard P, Barnes A, Bailey AJ et al. 2012. Brain anatomy and its relationship to behavior in adults with autism spectrum disorder: a multicenter magnetic resonance imaging study. Arch Gen Psychiatry. 69:195–209.
Filippini N, MacIntosh BJ, Hough MG, Goodwin GM, Frisoni GB, Smith SM, Matthews PM, Beckmann CF, Mackay CE. 2009. Distinct patterns of brain activity in young carriers of the APOE-epsilon4 allele. Proc Natl Acad Sci USA. 106:7209–7214.
Fox MD, Zhang D, Snyder AZ, Raichle ME. 2009. The global signal and observed anticorrelated resting state brain networks. J Neurophysiol. 101:3270–3283.
Garber K. 2007. Neuroscience. Autism's cause may reside in abnormalities at the synapse. Science. 317:190–191.
Geschwind DH. 2011. Genetics of autism spectrum disorders. Trends Cogn Sci. 15:409–416.
Glessner JT, Wang K, Cai G, Korvatska O, Kim CE, Wood S, Zhang H, Estes A, Brune CW, Bradfield JP et al. 2009. Autism genome-wide copy number variation reveals ubiquitin and neuronal genes. Nature. 459:569–573.
Gotts SJ, Simmons WK, Milbury LA, Wallace GL, Cox RW, Martin A. 2012. Fractionation of social brain circuits in autism spectrum disorders. Brain. 135:2711–2725.
Greicius MD, Krasnow B, Reiss AL, Menon V. 2003. Functional connectivity in the resting brain: a network analysis of the default mode hypothesis. Proc Natl Acad Sci USA. 100:253–258.
Herbert MR, Ziegler DA, Makris N, Filipek PA, Kemper TL, Normandin JJ, Sanders HA, Kennedy DN, Caviness VS Jr. 2004. Localization of white matter volume increase in autism and developmental language disorder. Ann Neurol. 55:530–540.
Hinsby AM, Kiemer L, Karlberg EO, Lage K, Fausboll A, Juncker AS, Andersen JS, Mann M, Brunak S. 2006. A wiring of the human nucleolus. Mol Cell. 22:285–295.
Jennings RG, Van Horn JD. 2012. Publication bias in neuroimaging research: implications for meta-analyses. Neuroinformatics. 10:67–80.
Joel SE, Caffo BS, van Zijl PC, Pekar JJ. 2011. On the relationship between seed-based and ICA-based measures of functional connectivity. Magn Reson Med. 66:644–657.
Johnson RT, Dickersin K. 2007. Publication bias against negative results from clinical trials: three of the seven deadly sins. Nat Clin Pract Neurol. 3:590–591.
Just MA, Cherkassky VL, Keller TA, Kana RK, Minshew NJ. 2007. Functional and anatomical cortical underconnectivity in autism: evidence from an FMRI study of an executive function task and corpus callosum morphometry. Cereb Cortex. 17:951–961.
Just MA, Cherkassky VL, Keller TA, Minshew NJ. 2004. Cortical activation and synchronization during sentence comprehension in high-functioning autism: evidence of underconnectivity. Brain. 127:1811–1821.
Kelly RE Jr, Alexopoulos GS, Wang Z, Gunning FM, Murphy CF, Morimoto SS, Kanellopoulos D, Jia Z, Lim KO, Hoptman MJ. 2010. Visual inspection of independent components: defining a procedure for artifact removal from fMRI data. J Neurosci Methods. 189:233–245.
Kennedy DP, Courchesne E. 2008. The intrinsic functional organization of the brain is altered in autism. Neuroimage. 39:1877–1885.
Kleinhans NM, Richards T, Sterling L, Stegbauer KC, Mahurin R, Johnson LC, Greenson J, Dawson G, Aylward E. 2008. Abnormal functional connectivity in autism spectrum disorders during face processing. Brain. 131:1000–1012.
Koshino H, Carpenter PA, Minshew NJ, Cherkassky VL, Keller TA, Just MA. 2005. Functional connectivity in an fMRI working memory task in high-functioning autism. Neuroimage. 24: 810–821.
Koshino H, Kana RK, Keller TA, Cherkassky VL, Minshew NJ, Just MA. 2008. fMRI investigation of working memory for faces in autism: visual coding and underconnectivity with frontal areas. Cereb Cortex. 18:289–300.
Lee M, Martin-Ruiz C, Graham A, Court J, Jaros E, Perry R, Iversen P, Bauman M, Perry E. 2002. Nicotinic receptor abnormalities in the cerebellar cortex in autism. Brain. 125:1483–1495.
Levitt P, Campbell DB. 2009. The genetic and neurobiologic compass points toward common signaling dysfunctions in autism spectrum disorders. J Clin Invest. 119:747–754.
Lin A, Tsai K, Rangel A, Adolphs R. 2012. Reduced social preferences in autism: evidence from charitable donations. J Neurodevel Disord. 4:8.
Lord C, Risi S, Lambrecht L, Cook EH Jr, Leventhal BL, DiLavore PC, Pickles A, Rutter M. 2000. The autism diagnostic observation schedule-generic: a standard measure of social and communication deficits associated with the spectrum of autism. J Autism Dev Disord. 30:205–223.
Lord C, Rutter M, Le Couteur A. 1994. Autism Diagnostic Interview-Revised: a revised version of a diagnostic interview for caregivers of individuals with possible pervasive developmental disorders. J Autism Dev Disord. 24:659–685.
MacKenzie-Graham A, Boline J, Toga AW. 2007. Brain atlases and neuroanatomic imaging. Methods Mol Biol. 401:183–194.

Madsen KM, Lauritsen MB, Pedersen CB, Thorsen P, Plesner AM, Andersen PH, Mortensen PB. 2003. Thimerosal and the occurrence of autism: negative ecological evidence from Danish population-based data. Pediatrics. 112:604–606.
Madsen KM, Lauritsen MB, Pedersen CB, Thorsen P, Plesner AM, Andersen PH, Mortensen PB. 2004. [Thimerosal and the occurrence of autism. Negative ecological evidence from Danish registry-data]. Ugeskr Laeger. 166:3291–3293.
Mazaika PK, Whitfield S, Cooper JC. 2005. Detection and repair of transient artifacts in fMRI data. Toronto, Canada: Human Brain Mapping. 581 p.
Minshew NJ, Williams DL. 2007. The new neurobiology of autism: cortex, connectivity, and neuronal organization. Arch Neurol. 64:945–950.
Monk CS, Peltier SJ, Wiggins JL, Weng SJ, Carrasco M, Risi S, Lord C. 2009. Abnormalities of intrinsic functional connectivity in autism spectrum disorders. Neuroimage. 47:764–772.
Muller RA, Shih P, Keehn B, Deyoe JR, Leyden KM, Shukla DK. 2011. Underconnected, but how? A survey of functional connectivity MRI studies in autism spectrum disorders. Cereb Cortex. 21:2233–2243.
Perry W, Minassian A, Lopez B, Maron L, Lincoln A. 2007. Sensorimotor gating deficits in adults with autism. Biol Psychiatry. 61:482–486.
Power JD, Barnes KA, Snyder AZ, Schlaggar BL, Petersen SE. 2012. Spurious but systematic correlations in functional connectivity MRI networks arise from subject motion. Neuroimage. 59:2142–2154.
Rademacher J, Galaburda AM, Kennedy DN, Filipek PA, Caviness VS. 1992. Human cerebral cortex - localization, parcellation, and morphometry with magnetic-resonance-imaging. J Cogn Neurosci. 4:352–374.
Sbacchi S, Acquadro F, Calo I, Cali F, Romano V. 2010. Functional annotation of genes overlapping copy number variants in autistic patients: focus on axon pathfinding. Curr Genomics. 11:136–145.
Shirer WR, Ryali S, Rykhlevskaia E, Menon V, Greicius MD. 2012. Decoding subject-driven cognitive states with whole-brain connectivity patterns. Cereb Cortex. 22:158–165.
Smith SM, Fox PT, Miller KL, Glahn DC, Fox PM, Mackay CE, Filippini N, Watkins KE, Toro R, Laird AR et al. 2009. Correspondence of the brain's functional architecture during activation and rest. Proc Natl Acad Sci USA. 106:13040–13045.
State MW, Levitt P. 2011. The conundrums of understanding genetic risks for autism spectrum disorders. Nat Neurosci. 14:1499–1506.
Stevens WD, Buckner RL, Schacter DL. 2010. Correlated low-frequency BOLD fluctuations in the resting human brain are modulated by recent experience in category-preferential visual regions. Cereb Cortex. 20:1997–2006.
Tyszka JM, Kennedy DP, Adolphs R, Paul LK. 2011. Intact bilateral resting-state networks in the absence of the corpus callosum. J Neurosci. 31:15154–15162.
Van Dijk KR, Hedden T, Venkataraman A, Evans KC, Lazar SW, Buckner RL. 2010. Intrinsic functional connectivity as a tool for human connectomics: theory, properties, and optimization. J Neurophysiol. 103:297–321.
Van Dijk KR, Sabuncu MR, Buckner RL. 2012. The influence of head motion on intrinsic functional connectivity MRI. Neuroimage. 59:431–438.
Veenstra-VanderWeele J, Muller CL, Iwamoto H, Sauer JE, Owens WA, Shah CR, Cohen J, Mannangatti P, Jessen T, Thompson BJ et al. 2012. Autism gene variant causes hyperserotonemia, serotonin receptor hypersensitivity, social impairment and repetitive behavior. Proc Natl Acad Sci USA. 109:5469–5474.
von dem Hagen EA, Nummenmaa L, Yu R, Engell AD, Ewbank MP, Calder AJ. 2011. Autism spectrum traits in the typical population predict structure and function in the posterior superior temporal sulcus. Cereb Cortex. 21:493–500.
von dem Hagen EA, Stoyanova RS, Baron-Cohen S, Calder AJ. 2012. Reduced functional connectivity within and between "social" resting state networks in autism spectrum conditions. Soc Cogn Affect Neurosci. [Epub ahead of print].
Waites AB, Stanislavsky A, Abbott DF, Jackson GD. 2005. Effect of prior cognitive state on resting state networks measured with functional connectivity. Hum Brain Mapp. 24:59–68.
Weinstein M, Ben-Sira L, Levy Y, Zachor DA, Ben Itzhak E, Artzi M, Tarrasch R, Eksteine PM, Hendler T, Ben Bashat D. 2011. Abnormal white matter integrity in young children with autism. Hum Brain Mapp. 32:534–543.
Weng SJ, Wiggins JL, Peltier SJ, Carrasco M, Risi S, Lord C, Monk CS. 2010. Alterations of resting state functional connectivity in the default network in adolescents with autism spectrum disorders. Brain Res. 1313:202–214.
Zhang Y, Brady M, Smith S. 2001. Segmentation of brain MR images through a hidden Markov random field model and the expectation-maximization algorithm. IEEE Trans Med Imaging. 20:45–57.